Magnetic field induced 3D–1D crossover in type-II superconductors



2008 J. Phys.: Condens. Matter 20 423201

(http://iopscience.iop.org/0953-8984/20/42/423201)

J. Phys.: Condens. Matter **20** (2008) 423201 (15pp) doi:10.1088/0953-8984/20/42/423201

## TOPICAL REVIEW

# Magnetic field induced 3D–1D crossover in type-II superconductors

**T Schneider**

Physik-Institut der Universität Zürich, Winterthurerstrasse 190, CH-8057 Zürich, Switzerland

E-mail: tschnei@physik.unizh.ch

Received 11 March 2008, in final form 23 June 2008
Published 9 September 2008
Online at stacks.iop.org/JPhysCM/20/423201

**Abstract**

We review and analyze magnetization and specific heat investigations on type-II superconductors which uncover remarkable evidence for a magnetic field induced finite size effect, and an associated 3D–1D crossover which enhances thermal fluctuations. Indeed, the correlation length transverse to the magnetic field $H_i$, applied along the $i$-axis, cannot grow beyond the limiting magnetic length $L_{H_i} = (\Phi_0/(aH_i))^{1/2}$, related to the average distance between vortex lines. Noting that 1D is incompatible with the occurrence of a continuous phase transition at finite temperatures, we replace the mean-field transition line $H_{c2}(T)$ by the 3D–1D crossover line $H_p(T)$. Since the magnetic field induced finite size effect relies on thermal fluctuations, and their enhancement originating from the 3D–1D crossover, its observability is not restricted to just type-II superconductors with small correlation volume, including $YBa_2Cu_4O_8$, $NdBa_2Cu_3O_{7-\delta}$, $YBa_2Cu_3O_{7-\delta}$, and $DyBa_2Cu_3O_{7-\delta}$, where 3D $xy$ critical behavior has already been observed in zero field. Indeed, our analysis of the reversible magnetization of $RbOs_2O_6$ and the specific heat of $Nb_{77}Zr_{23}$, $Nb_3Sn$ and $NbSe_2$ reveals that even in these low $T_c$ superconductors with comparatively large correlation volume the 3D to 1D crossover is observable in sufficiently high magnetic fields. Consequently, below $T_c$ and above $H_{pi}(T)$ superconductivity is confined to cylinders with diameter $L_{H_i}$ (1D) and there is no continuous phase transition in the $(H, T)$-plane along the $H_{c2}(T)$-line as predicted by the mean-field treatment. Moreover, we observe that a thermodynamic vortex melting transition occurs in the 3D regime. While in $YBa_2Cu_4O_8$, $NdBa_2Cu_3O_{7-\delta}$, $YBa_2Cu_3O_{7-\delta}$, and $DyBa_2Cu_3O_{7-\delta}$ it turns out to be driven by 3D $xy$ thermal fluctuations, the specific heat data for the conventional type-II superconductors $Nb_{77}Zr_{23}$, $Nb_3Sn$ and $NbSe_2$ point to Gaussian fluctuations. Because the vortex melting and the 3D–1D crossover line occur at universal values of the scaling variable their relationship is universal.

(Some figures in this article are in colour only in the electronic version)

## Contents



## 1. Introduction

The phenomenology of superconductivity is based on the Ginzburg–Landau theory [1], which provides the starting functional for the free energy for the charged superconductor, coupled to electromagnetism. The two fields determining the physics of the system are the superconducting order parameter $\Psi$ and the vector potential $\mathbf{A}$. In its simplest version, the order parameter, $\Psi = |\Psi| \exp(i\varphi)$, is a complex scalar. The resulting mean-field phase diagram was constructed by Abrikosov in

 

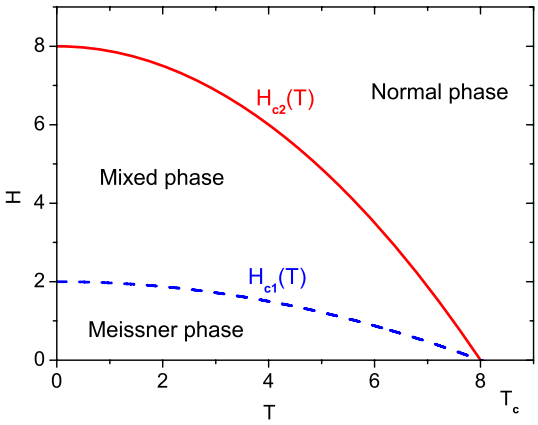


**Figure 1.** Mean-field phase diagram comprising a normal metallic phase at high fields and temperatures, separated by the upper critical field line $H_{c2}(T)$ from the mixed phase, which in turn is separated by the lower critical field line $H_{c1}(T)$ from the Meissner–Ochsenfeld phase at low temperatures and fields.

1957 [2] and provided a rather accurate description for all conventional superconductors. This mean-field $H$–$T$ phase diagram of a type-II superconductor is shown schematically in figure 1. It comprises a Meissner phase characterized by complete flux expulsion at low magnetic fields ($H < H_{c1}$), separated from the mixed phase at higher fields ($H > H_{c1}$), where the magnetic field penetrates the superconductor in the form of flux lines. The lower critical field $H_{c1}(T)$ depends on the London penetration depth $\lambda$, which is the length scale determining the electromagnetic response of the superconductor. Since the superconducting state is a macroscopic quantum fluid, the magnetic flux enclosed in a vortex is quantized in units of $\Phi_0 = hc/2e$, the flux quantum. With increasing field the density of flux lines, forming a triangular lattice, increases until the vortex cores overlap when the upper critical field $H_{c2}$ is reached. Above this field the normal metallic phase is recovered. The upper critical field $H_{c2}$ is determined by the correlation length of the superconductor, which is the second fundamental length scale in the system determining what is the characteristic distance for variations of the order parameter.

Going beyond this traditional mean-field picture, an obvious generalization amounts to including thermal fluctuations and disorder. Indeed, there is considerable experimental evidence for a melting transition transforming the vortex solid into a vortex liquid phase [3]. Such a melting transition can be understood in terms of thermal fluctuations in the phase $\varphi(r)$ of the order parameter $\Psi(r) = |\Psi(r)| \exp[i\varphi(r)]$. However, in the high field regime the phase diagram of cuprate superconductors in the $H$–$T$-plane is fixed by the interplay of thermal fluctuations and disorder [3–5]. Furthermore, as noted by Lee and Shenoy [6], the fluctuations of a type-II bulk superconductor in a magnetic field become effectively one dimensional and the superconductor behaves like an array of rods with diameter $L_H \propto H^{-1/2}$ perpendicular to the applied field. As a consequence the correlation length transverse to the applied field cannot grow beyond the limiting magnetic length $L_H$ and the superconductor undergoes with increasing field a 3D–1D crossover. Since fluctuations become more important with reduced dimensionality and there is a limiting magnetic length scale $L_H$, it becomes clear that the upper critical field $H_{c2}$ is an artifact of the approximations. Indeed, calculations of the specific heat in a magnetic field which treat the interaction terms in the Hartree approximation, and extensions thereof, find that the specific heat is smooth through the mean-field transition temperature $T_{c2}(H)$ [7–9]. In the context of finite size scaling this is simply due to the fact that the correlation length of fluctuations which are transverse to the applied magnetic field are bounded by the magnetic length $L_H \propto H^{-1/2}$.

In this article we review and analyze magnetization and specific heat investigations on type-II superconductors which uncover remarkable evidence for a magnetic field induced finite size effect, and an associated 3D–1D crossover which enhances the thermal fluctuations. Noting that 1D is incompatible with the occurrence of a continuous phase transition at finite temperatures, we replace the mean-field transition line $H_{c2}(T)$ by the 3D–1D crossover line $H_p(T)$. Along this line the correlation length transverse to the applied magnetic field attains the limiting magnetic length $L_H$ and for this reason there is no continuous phase transition. Since the magnetic field induced finite size effect relies on thermal fluctuations and their enhancement originating from the 3D to 1D crossover, the observability of the magnetic field induced finite size effect should not be restricted to type-II superconductors with small correlation volume only. In these systems, including $YBa_2Cu_4O_8$ [10], $NdBa_2Cu_3O_{7-\delta}$ [11], $YBa_2Cu_3O_{7-\delta}$ [12, 13], and $DyBa_2Cu_3O_{7-\delta}$ [14], 3D $xy$ critical behavior has been observed already in zero field. In addition, magnetization measurements on clean and untwinned $YBa_2Cu_3O_{6.95}$ single crystals with extremely low pinning uncovered the dominant role of thermal 3D $xy$ fluctuations in the vortex melting transition [15, 16]. Indeed, our analysis of the reversible magnetization of $RbOs_2O_6$ [17] and the specific heat of $Nb_{77}Zr_{23}$ [18], $Nb_3Sn$ [19] and $NbSe_2$ [20] reveals that even in these low $T_c$ superconductors with comparatively large correlation volume the 3D–1D crossover is observable in sufficiently high magnetic fields. In this context it should be kept in mind that the magnetic field induced enhancement of Gaussian fluctuations was also observed many years ago by Farrant and Gough [21] in Nb, and interpreted by Thouless [7] in terms of the magnetic field induced 3D–1D crossover. Moreover, we observe that the thermodynamic vortex melting transition occurs in the 3D regime. While in $YBa_2Cu_4O_8$, $NdBa_2Cu_3O_{7-\delta}$, $YBa_2Cu_3O_{7-\delta}$, and $DyBa_2Cu_3O_{7-\delta}$ it turns out to be driven by 3D $xy$ thermal fluctuations, the specific heat data for the conventional type-II superconductors $Nb_{77}Zr_{23}$, $Nb_3Sn$ and $NbSe_2$ point to Gaussian fluctuations. Because the vortex melting and the 3D–1D crossover line occur at universal values of the scaling variable, their relationship is universal.

## 2. Scaling and the magnetic field induced finite size effect

Next we sketch the scaling properties of the fluctuation contribution to the free energy per unit volume for a type-II superconductor in the presence of a magnetic field. On

this basis we establish the equivalence with a superfluid constrained to a cylinder which unavoidably undergoes a 3D–1D crossover. Invoking a Maxwell relation we then derive the scaling properties of the magnetization and specific heat near the 3D–1D crossover line. We are then prepared for analyzing the specific heat and reversible magnetization data for $YBa_2Cu_4O_8$ [10], $NdBa_2Cu_3O_{7-\delta}$ [11], $YBa_2Cu_3O_{7-\delta}$ [12, 13], and $DyBa_2Cu_3O_{7-\delta}$ [14], where critical fluctuations have been observed already in the zero-field transition. Subsequently we analyze the reversible magnetization of $RbOs_2O_6$ [17] and the specific heat of $Nb_{77}Zr_{23}$ [18], $Nb_3Sn$ [19] and $NbSe_2$ [20], type-II superconductors with comparatively large correlation volume, to explore the associated enhancement of thermal fluctuations due to the 3D–1D crossover.

It is well known that systems of finite extent, i.e. isolated superconducting grains, undergo a rounded and smooth phase transition [22]. As in an infinite and homogeneous system, the transition temperature $T_c$ is approached, the correlation length $\xi$ increases strongly, and it diverges at $T_c$. However, in real systems the increase of the correlation length is limited by the spatial extent $L_i$ of the homogeneous domains in direction $i$. In type-II superconductors, exposed to a magnetic field $H_i$, there is an additional limiting length scale $L_{H_i} = \sqrt{\Phi_0/(aH_i)}$ with $a \simeq 3.12$ [23], related to the average distance between vortex lines [23–26]. Indeed, as the magnetic field increases, the density of vortex lines becomes greater, but this cannot continue indefinitely; the limit is roughly set, on the proximity of vortex lines, by the overlapping of their cores. Due to these limiting length scales the phase transition is rounded and occurs smoothly. Indeed, approaching $T_c$ from above, the correlation length $\xi_i$ in direction $i$ increase strongly. However, due to the limiting length scales $L_i$ and $L_{H_i} = \sqrt{\Phi_0/(aH_i)}$, it is bounded and cannot grow beyond [23]

$$\begin{aligned}
&\xi_i\left(T_p\left(L_i\right)\right) = \xi_{0i}^{-}\left|t_{pL}\right|^{-\nu} = L_i,\\
&\sqrt{\xi_i\left(T_p\left(H_k\right)\right)\xi_j\left(T_p\left(H_k\right)\right)} = \sqrt{\xi_{0i}^{-}\xi_{0j}^{-}}\left|t_p\left(H_k\right)\right|^{-\nu} \qquad (1)\\
&= \sqrt{\Phi_0/\left(aH_k\right)} = L_{H_k}, \qquad i \neq j \neq k,
\end{aligned}$$

where

$$t = T/T_c - 1. \qquad (2)$$

$\nu$ denotes the critical exponent of the correlation lengths $\xi_i$ with critical amplitude $\xi_{0i}^{-}$ below $T_c$.

To explore the evidence for the occurrence of these finite size effects we concentrate on the behavior of the magnetization and the specific heat below the zero-field transition temperature $T_c$. Our starting point is the fluctuation contribution to the free energy per unit volume. In the presence of a magnetic field applied parallel to the $c$-axis it adopts the scaling form [23, 26–28]

$$f_s = \frac{Q^{-}k_B T}{\xi_{ab}^2\xi_c}G\left(z\right), \qquad z = \frac{\xi_{ab}^2 H_c}{\Phi_0}, \qquad (3)$$

where $G(z)$ is a universal scaling function of its argument, $Q^{-}$ a universal constant and $H_c$ denotes the magnetic field applied along the $c$-axis. For a brief derivation of the resulting universal relations and scaling forms for the magnetization and specific heat we refer the reader to the appendix. The scaling function $G(z)$ is expected to exhibit a singularity at the universal value $z_m$ of the scaling variable $z$, which describes the thermodynamic vortex melting line [28]

$$t_m = \left(\frac{(\xi_{ab0}^{-})^2 H_c}{\Phi_0 z_m}\right)^{1/2\nu}. \qquad (4)$$

There is considerable evidence that the vortex lattice melts in very clean samples via a first-order phase transition [29–31]. With the introduction of random vortex pinning defects, however, the first-order melting transition becomes more continuous [29, 32–34]; this is commonly referred to as the 'vortex glass' transition. There is evidence for different glassy phases (Bose glass, Bragg glass and vortex glass) [29], the detailed nature of which appears to be controversial. In any case, in sufficiently clean systems there is a thermal fluctuation driven vortex melting transition. In this case it occurs at a universal value of the scaling variable, and relation (4) implies that the isotope and pressure effects on transition temperature, melting temperature and in-plane correlation length are not independent.

To recognize the implications of the magnetic field induced finite size effect, it is instructive to note that this scaling is formally equivalent to that of an uncharged superfluid, such as $^4$He, constrained to a cylinder of diameter $L_{H_c} = (\Phi_0/(aH_c))^{1/2}$. Indeed, the finite size scaling theory predicts that for a system confined to a barlike geometry, $LLH$ where $H \to \infty$, an observable $O(t, L)$ scales as [35–37]

$$\frac{O\left(t, L\right)}{O\left(t, \infty\right)} = f_O\left(y\right), \qquad y = \xi(t)/L, \qquad (5)$$

where $f(y)$ is the finite size scaling function. As in the confined system a 3D–1D crossover occurs, there is a rounded transition only. Indeed, because the correlation length $\xi(T)$ cannot grow beyond $L$ there is the 3D–1D crossover line

$$T_{pL} = T_c\left(1 - \left(\frac{\xi_0^{-}}{L}\right)^{1/\nu}\right), \qquad (6)$$

which transforms with equation (1) to

$$\begin{aligned}
T_p(H_c) &= T_c\left(1 - \left(\frac{\xi_{ab0}^{-}}{L_{H_c}}\right)^{1/2\nu}\right)\\
&= T_c\left(1 - \left(\frac{aH_c\left(\xi_{ab0}^{-}\right)^2}{\Phi_0}\right)^{1/2\nu}\right) \qquad (7)
\end{aligned}$$

in the magnetic field induced case. In this context it should be recognized that 1D systems with short range interactions do not undergo a continuous phase transition at finite temperature [38]. To uncover this crossover line we invoke Maxwell's relation $\partial(C/T)/\partial H_c|_T = \partial^2 M/\partial T^2|_{H_c}$. Together with the scaling forms of specific heat and magnetization, this yields the relation (equation (A.13))

$$\begin{aligned}
&T H_c^{1+\alpha/2\nu}\frac{\partial(c/T)}{\partial H_c} = T H_c^{1+\alpha/2\nu}\frac{\partial^2 m}{\partial T^2}\\
&= -\frac{k_B A^{\pm}}{2\alpha\nu}\left|x\right|^{1-\alpha}\frac{\partial f_c^{\pm}}{\partial x}, \qquad (8)
\end{aligned}$$

where $m = M/V$ is the magnetization per unit volume. Accordingly, magnetization and specific heat data taken in different fields and plotted as $H_c^{1+\alpha/2\nu}\partial^2 m/\partial T^2$ versus $x = t/H_c^{1/2\nu}$ and $H^{(1+\alpha)/2\nu}\partial(C/T)/\partial H_c$ versus $t/H^{1/2\nu}$ should then collapse onto a single curve, separately. Note that this scaling form applies as long as the limiting length is set by the magnetic field in the form $L_{H_c} = \sqrt{\Phi_0/(aH_c)}$. However, for real type-II superconductors the spatial extent $L_{ab}$ of the homogeneous domains is limited and, on lowering the applied magnetic field $L_{H_c}$, approaches $L_{ab}$ unavoidably. In the regime where the growth of the in-plane correlation length is limited by $L_{H_c}$, these plots are expected to uncover the vortex melting transition line in the form of a peak at $x_m$ and the 3D–1D crossover line in the form of a dip at $x_p$. This dip replaces the singularity at the so-called upper critical field resulting from the Gaussian approximation and the neglect of the magnetic field induced finite size effect (see (A.19)).

Another suitable observable for uncovering the magnetic field induced crossover is the derivative of the specific heat with respect to temperature. According to equation (A.14) it adopts the scaling form

$$\frac{\mathrm{d}c}{\mathrm{d}T} = \frac{A^-}{T_c} H_c^{-(1+\alpha)/2\nu}\left(x^{-(1+\alpha)/2\nu} f(x) - \alpha x^{-\alpha}\frac{\mathrm{d}f}{\mathrm{d}x}\right), \quad (9)$$

whereby the data $\mathrm{d}c/\mathrm{d}T$ for different fields should collapse onto a single curve when plotted as $H_c^{(1+\alpha)/2\nu} T_c\, \mathrm{d}c/\mathrm{d}T$ versus $tH_c^{-1/2\nu}$. In the regime where the growth of the in-plane correlation length is limited by $L_{H_c}$ this plot should also uncover the vortex melting transition line in the form of a peak at $x_m$ and the 3D to 1D crossover line in the form of a dip at $x_p$. This dip replaces the singularity at the so-called upper critical field resulting from the Gaussian approximation and the neglect of the magnetic field induced finite size effect (see (A.22)).

There is considerable evidence that cuprate superconductors with moderate anisotropy exhibit, in zero field, 3D $xy$ critical behavior [11–14, 23, 25–27, 39–47]. The critical exponents are then given by [48, 49]

$$\alpha = 2\nu - 3 \simeq -0.013, \qquad \nu \simeq 0.671 \simeq 2/3. \quad (10)$$

As disorder is concerned, there is the Harris criterion [50], which states that short range correlated and uncorrelated disorder is irrelevant at the unperturbed critical point, provided that the specific heat exponent $\alpha$ is negative. However, when superconductivity is restricted to homogeneous domains of finite spatial extent $L_{ab,c}$, the system is inhomogeneous and the resulting rounded transition uncovers a finite size effect [35–37] because the correlation lengths $\xi_{ab,c} = \xi^{\pm}_{ab0,c0}|t|^{-\nu}$ cannot grow beyond $L_{ab,c}$, the respective extent of the homogeneous domains. Hence, as long as $\xi_{ab,c} < L_{ab,c}$, the critical properties of the fictitious homogeneous system can be explored. There is considerable evidence that this scenario accounts for the rounded transition seen in the specific heat [27] and the magnetic penetration depths [46] in zero field. Nevertheless, as long as $L_{H_k} < L_i$, the magnetic field induced finite size effect sets the limiting length scale, and the scaling plots $T H_c^{1+\alpha/2\nu}\partial^2 m/\partial T^2$ versus $x = t/H_c^{1/2\nu}$ and

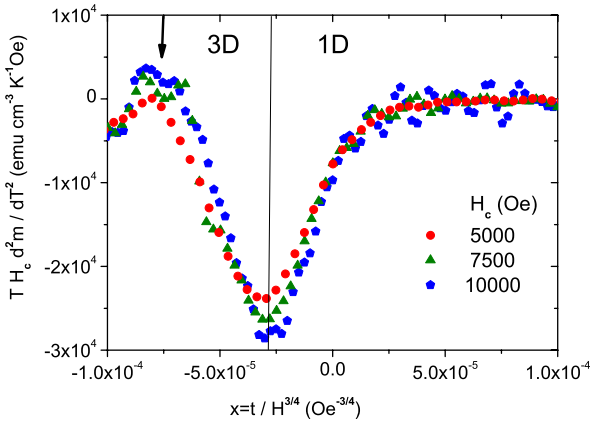


**Figure 2.** $T H_c\, \mathrm{d}^2 m/\mathrm{d}T^2$ versus $x = t/H_c^{3/4}$ for a $YBa_2Cu_4O_8$ single crystal with $T_c \simeq 79.6$ K, taken from Weyeneth *et al* [10]. The arrow marks the melting line $x_m \simeq -7.5 \times 10^{-5}$ $Oe^{-3/4}$ and the vertical line $x_p \simeq -2.85 \times 10^{-5}$ $Oe^{-3/4}$ the 3D to 1D crossover line.

$T H^{(1+\alpha)/2\nu}\, \mathrm{d}(C/T)/\mathrm{d}T$ versus $t/H^{1/2\nu}$ should uncover the collapse onto a single curve.

In classic superconductors, such as $Nb_{77}Zr_{23}$, $Nb_3Sn$ and $NbSe_2$, the zero-field specific heat measurements uncover near $T_c$ remarkable consistency with the standard mean-field jump [18–20]. According to this it is unlikely that the magnetic field induced 3D to 1D crossover is associated with 3D $xy$ thermal fluctuations. Here we consider the contribution of Gaussian fluctuations limited by the magnetic field induced finite size effect. In this case the outlined scaling forms apply as well, but the critical exponents are given by [27, 49]

$$\alpha = 1/2, \qquad \nu = 1/2. \quad (11)$$

## 3. Analysis of experimental data

We are now prepared to review and analyze experimental data to explore the occurrence of the magnetic field induced finite size effect and the associated 3D–1D crossover. In figure 2 we depict the scaling plot $T H_c\, \mathrm{d}^2 m/\mathrm{d}T^2$ versus $t H_c^{-3/4}$ for a $YBa_2Cu_4O_8$ single crystal taken from Weyeneth *et al* [10]. It corresponds to equation (8) with the 3D $xy$ exponents (equation (10)). Apparently, the data collapse reasonably well onto a single curve, consistently with dominant 3D $xy$ fluctuations. The occurrence of a dip and the peak, marked by the vertical line and the arrow, respectively, differ drastically from the mean-field behavior where $\partial^2 m/\partial T^2 = 0$. Moreover, the finite depth contradicts the reputed singularity at $T_{c2}$ obtained in the Gaussian approximation [51]. The observed collapse of the data onto a single curve reveals consistency with 3D $xy$ fluctuations down to $H_c = 5 \times 10^3$ Oe, limited by the magnetic field induced finite size effect only. From $L_{H_c} = (\Phi_0/(aH_c))^{1/2}$, $a \simeq 3.12$ and $H_c = 5 \times 10^3$ Oe, we obtain for the extent of the homogeneous domains the lower bound $L_{ab} > 3.6 \times 10^{-4}$ cm. In figure 3, we depict the scaling plot $m/(T H_c^{1/2})$ versus $t/H^{3/4}$ for $YBa_2Cu_4O_8$, where the magnetization data fall on a single curve (equation (A.1)) when 3D $xy$ fluctuations dominate. It is readily seen that in this plot signatures of the peak and dip structure in $T H_c\, \mathrm{d}^2 m/\mathrm{d}T^2$

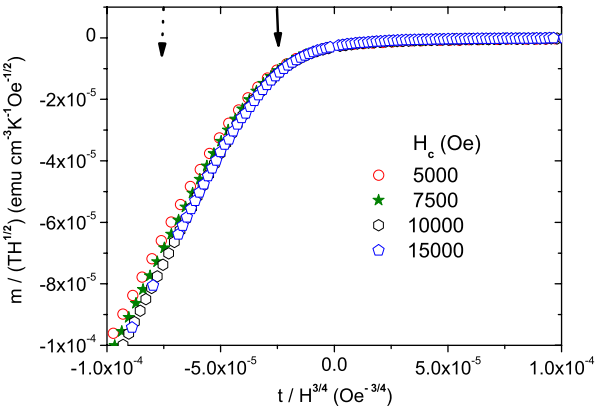


**Figure 3.** $m/(T H_c^{1/2})$ versus $t/H^{3/4}$ for a $YBa_2Cu_4O_8$ single crystal taken from [10] for magnetic fields $H_c$ applied along the $c$-axis. The arrows mark the melting (↓) and the 3D to 1D crossover line (↓).

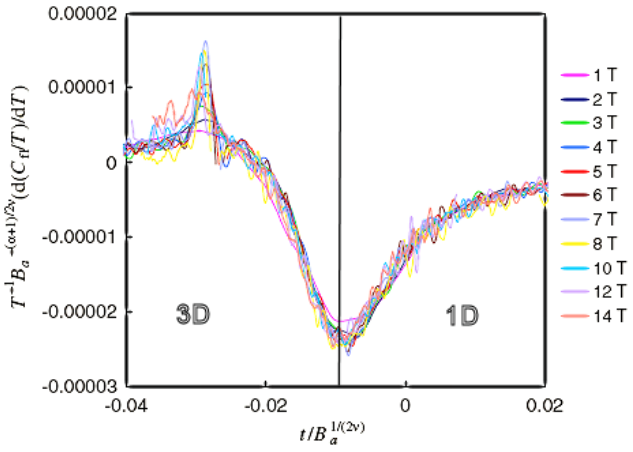


**Figure 4.** Scaling plot $T^{-1}H^{(1+\alpha)/2\nu}\,\mathrm{d}(C/T)/\mathrm{d}T$ versus $t/H^{1/2\nu}$ for a $NdBa_2Cu_3O_{7-\delta}$ single crystal with $T_c = 95.5$ K taken from Plackowski *et al* [11]. Units are teslas, joules per gram atom and kelvins. The vertical line marks the 3D to 1D crossover line equation (18) separating the 3D from the 1D regime.

versus $x = t/H_c^{3/4}$ are hardly visible. Though this plot reveals the dominant critical fluctuations it does not provide further insight. To relate the finite depth of the dip and the magnetic field induced finite size effect we note that at $T_p(H_c)$ the in-plane correlation length $\xi_{ab}$ attains according to equation (1) the limiting magnetic length $L_{H_c}$, so

$$\xi_{ab}(T_p) = \xi_{ab0}^{-}\left|t_p\,(H_c)\right|^{-\nu} = L_{H_c} = \left(\frac{\Phi_0}{a H_c}\right)^{1/2}. \qquad (12)$$

At $T_p$, equation (8) yields

$$\left.\frac{\partial^2 m}{\partial T^2}\right|_{T=T_p(H_c)} = -\frac{k_B A^{\pm}}{2\alpha\nu T} H_c^{-1-\alpha/2\nu}\,|x|^{1-\alpha}\left.\frac{\partial f_c^{\pm}}{\partial x}\right|_{T=T_p(H_c)}$$
$$= -\frac{k_B A^{\pm}}{2\alpha\nu T}\,|x|^{1-\alpha}\,\frac{\partial f_c^{\pm}}{\partial x}\left(\frac{a\xi_{ab}^2(T)}{\Phi_0}\right)^{1+\alpha/2\nu}\Bigg|_{T=T_p(H_c)}, \qquad (13)$$

revealing that the depth of the dip in $\partial^2 m(H_c,T)/\partial T^2$ versus $T$ is controlled by the limited growth of the in-plane correlation length $\xi_{ab}$. This differs drastically from the Gaussian approximation where $\partial^2 m(H_c,T)/\partial T^2$ diverges at the so-called upper critical field because the limited growth of the correlation length is not taken into account (see the appendix). As $\xi_{ab}$ attains $T_p(H_c)$ the limiting magnetic length $L_{H_c}$, $\partial m(H_c,T)/\partial T$ versus $T$ exhibits for fixed $H_c$ an inflection point and for $\partial^2 m(H_c,T)/\partial T^2$ an extremum. Accordingly,

$$t_p(H_c)H_c^{-3/4} = -2.85\times10^{-5}\left(\mathrm{Oe}^{-3/4}\right), \qquad (14)$$

determines the 3D–1D crossover line along which $\xi_{ab} = L_{H_c}$. Moreover, there is a peak in the 3D regime at

$$t_m(H_c)H_c^{-3/4} \simeq -8.35\times10^{-5}\left(\mathrm{Oe}^{-3/4}\right), \qquad (15)$$

signaling the vortex melting transition (equation (4)). Indeed, rewritten in the form $H_{mc} \simeq 2.7\times10^5(1-T_m/T_c)^{4/3}$ (Oe), this agrees reasonably well with the previous estimate $H_{mc} \simeq 1.8\times10^5(1-T_m/T_c)^{4/3}$ (Oe) of Katayama *et al* [52]. Combining our estimates for the vortex melting and 3D–1D crossover line we obtain for the universal ratios between the respective values of the scaling variables and the reduced temperatures the estimates

$$\frac{z_m}{z_p} = \left(\frac{t_p(H_c)}{t_m\,(H_c)}\right)^{2\nu} \simeq 0.24, \qquad t_p(H_c)/t_m(H_c) \simeq 0.34, \qquad (16)$$

in reasonable agreement with the values listed in table 1 for $NdBa_2Cu_3O_{7-\delta}$, $YBa_2Cu_3O_{6.97}$, and $DyBa_2Cu_3O_{6.97}$. Another quantity, suitable for uncovering the vortex melting and the 3D–1D crossover line, is the derivative of the specific heat with respect to temperature. It adopts the scaling form (equation (A.21))

$$\frac{\mathrm{d}c}{\mathrm{d}T} = \frac{A^-}{T_c}H_c^{-(1+\alpha)/2\nu}\left(x^{-(1+\alpha)/2\nu}f(x) - \alpha x^{-\alpha}\frac{\mathrm{d}f}{\mathrm{d}x}\right). \qquad (17)$$

Thus, the data for different fields should collapse onto a single curve when plotted as $H_c^{(1+\alpha)/2\nu}T_c\,\mathrm{d}c/\mathrm{d}T$ versus $t\,H_c^{-1/2\nu}$.

In figure 4 we show the data of Plackowski *et al* [11] for a $NdBa_2Cu_3O_{7-\delta}$ single crystal with $T_c = 95.5$ K in the form $T^{-1}H_c^{(1+\alpha)/2\nu}\,\mathrm{d}(C/T)/\mathrm{d}T$ versus $t\,H_c^{-1/2\nu}$ with the 3D $xy$ exponents (equation (10)). Apparently, the data scale from 1 to 14 T remarkably well. An essential feature is the dip reaching its minimum at

$$t_p(H_c)H_c^{-3/4} \simeq -0.0087\left(\mathrm{T}^{-3/4}\right), \qquad (18)$$

which determines the 3D–1D crossover line. Indeed it replaces the singularity at the so-called upper critical field resulting

**Table 1.** Summary of the estimates for the universal ratio $z_m/z_p$, $t_p/t_m$, and the critical amplitude of the in-plane correlation length $\xi_{ab0}^{-}$ below $T_c$.

| | $z_m/z_p$ | $t_p/t_m$ | $\xi_{ab0}^{-}$ (Å) | $T_c$ (K) | Reference | Equation |
|---|---|---|---|---|---|---|
| $YBa_2Cu_4O_8$ | 0.24 | 0.34 | 15.6 | 79.6 | [10] | (16) |
| $NdBa_2Cu_3O_{7-\delta}$ | 0.2 | 0.3 | 24 | 95.5 | [11] | (23) |
| $YBa_2Cu_3O_{6.97}$ | 0.25 | 0.35 | 27 | 91.1 | [12] | (28) |
| $DyBa_2Cu_3O_{6.97}$ | 0.24 | 0.34 | 25 | 91.05 | [14] | (32) |

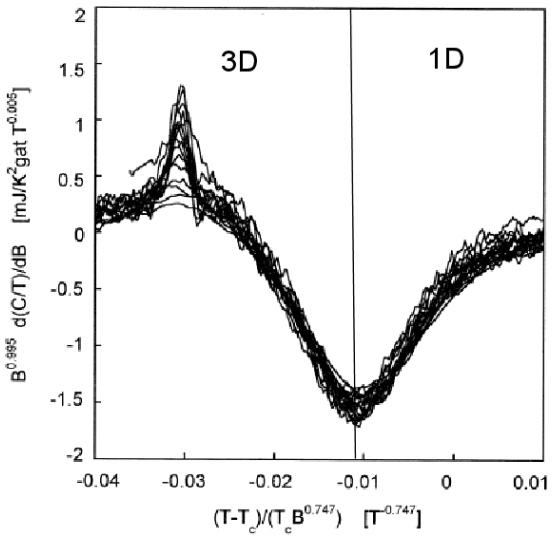


**Figure 5.** Scaling plot of $H_c^{1+\alpha/2\nu}\partial(C/T)/\partial H_c$ versus $tH_c^{-1/2\nu}$ for a $YBa_2Cu_3O_{6.97}$ single crystal with $T_c = 91.1$ K and $H_c = 1.75$, 2.25, 2.75, 3.25, 3.75, 4.25, 4.75, 5.25, 5.75, 6.25, 6.75, 7.25, 8, 9, 10, 11.25 and 13 T, taken from Roulin *et al* [12]. The solid line marks the 3D–1D crossover line (equation (25)).

from the Gaussian approximation and the neglect of the magnetic field induced finite size effect (see (A.22)). With equation (13) it yields for the critical amplitude of the in-plane correlation length the estimate

$$\xi_{ab0}^{-} \simeq 24\ \text{Å}. \tag{19}$$

Furthermore, combining equations (12) and (17) we obtain

$$\left.\frac{dc}{dT}\right|_{T=T_p(H_c)} = \frac{A^-}{T_c}\left(\frac{a\xi_{ab}^2(T)}{\Phi_0}\right)^{-\frac{1+\alpha}{2\nu}} \times \left(x^{-\frac{1+\alpha}{2\nu}} f(x) - \alpha x^{-\alpha}\frac{df}{dx}\right)\Bigg|_{T=T_p(H_c)}, \tag{20}$$

revealing that down to 1 T the depth of the dip is controlled by $\xi_{ab}(T_p(H_c)) = L_{H_c}$, the magnetic field induced limiting value of the in-plane correlation length. Accordingly, the homogeneous domains exceed $L_{ab} = (\Phi_0/aH_c)^{1/2} \simeq 2.6 \times 10^{-6}$ cm. In addition, in the 3D regime we observe a peak around

$$t_m(H_c)H_c^{-3/4} \simeq -0.029\left(\mathrm{T}^{-3/4}\right), \tag{21}$$

which was traced back to the vortex melting transition [11]. From

$$z_m = (\xi_{ab0}^{-})^2\,|t_m(H_c)|^{-2\nu}\,H_c/\Phi_0, \qquad z_p = (\xi_{ab0}^{-})^2\,|t_p(H_c)|^{-2\nu}\,H_c/\Phi_0, \tag{22}$$

and the estimates (18) and (21), the universal ratios of the scaling variables and the reduced temperatures at the melting transition and the 3D–1D crossover line adopt then the values

$$z_m/z_p = \left(t_p(H_c)/t_m(H_c)\right)^{2\nu} \simeq 0.2, \qquad t_p(H_c)/t_m(H_c) \simeq 0.3 \tag{23}$$

in reasonable agreement with the values listed in table 1 for $YBa_2Cu_4O_8$, $YBa_2Cu_3O_{6.97}$, and $DyBa_2Cu_3O_{6.97}$. With $z_p = 1/a \simeq 0.32$ the universal value of the scaling variable, $z_m = (\xi_{ab0}^{-})^2|t_m|^{-2\nu}H_c/\Phi_0$, at the melting transition is

$$z_m \simeq 0.06. \tag{24}$$

Hence, 3D $xy$ fluctuations do not determine just the 3D–1D crossover line, but determine the melting line, belonging to the 3D regime, as well.

In figure 5 we depict the scaling plot $H_c^{1+\alpha/2\nu}\partial(C/T)/\partial H_c$ versus $tH_c^{-1/2\nu}$ with 3D $xy$ exponents (equation (10)) for a $YBa_2Cu_3O_{6.97}$ single crystal, taken from Roulin *et al* [12]. The collapse of the data onto a single curve uncovers again consistency with 3D $xy$ fluctuations. Moreover, we observe that down to 1.75 T the depth of the dip is controlled by $\xi_{ab}(T_p(H_c)) = L_{H_c}$, the magnetic field induced limiting value of the in-plane correlation length. Accordingly, the homogeneous domains exceed $L_{ab} = (\Phi_0/aH_c)^{1/2} \simeq 1.9 \times 10^{-6}$ cm. The minimum of the dip at

$$t_p(H_c)H_c^{-1/2\nu} = -0.011\left(\mathrm{T}^{-3/4}\right), \tag{25}$$

determines the 3D–1D crossover line. With equation (12) it yields for the critical amplitude of the in-plane correlation length the estimate

$$\xi_{ab0}^{-} \simeq 27\ \text{Å}. \tag{26}$$

The rather sharp peak in the 3D regime at

$$t_m(H_c)H_c^{-3/4} \simeq -0.031\left(\mathrm{T}^{-3/4}\right), \tag{27}$$

uncovers again the vortex melting line. These estimates yield for the universal ratios the values

$$z_m/z_p = \left(t_p(H_c)/t_m(H_c)\right)^{2\nu} \simeq 0.25, \qquad t_p(H_c)/t_m\,(H_c) \simeq 0.35, \tag{28}$$

in reasonable agreement with the values listed in table 1 for $YBa_2Cu_4O_8$, $NdBa_2Cu_3O_{7-\delta}$, and $DyBa_2Cu_3O_{6.97}$. Recently it was shown that the melting line depends on the pressure [53]. The underlying coupling between the vortex transition and the crystal lattice then demonstrates that the crystal lattice is more than a mere host for the vortices. On the other hand, from the universal relation (4) it follows naturally that the relationship between $T_c$, $T_m$ and the in-plane correlation length is fixed. From this we anticipate that if $T_c$ is raised (lowered) by applying uniaxial pressure, the melting line will be shifted to higher (lower) temperatures.

In figure 6 we depict the scaling plot $H_c^{1+\alpha/2\nu}\partial(C/T)/\partial H_c$ versus $tH_c^{-1/2\nu}$ for a $DyBa_2Cu_3O_{7-x}$ single crystal, taken from Garfield *et al* [14]. It reveals again a reasonable collapse of the data onto a single curve and, with that, consistency with 3D $xy$ fluctuations. In addition we observe that down to 1.5 T the depth of the dip is controlled by $\xi_{ab}(T_p(H_c)) = L_{H_c}$, the magnetic field induced limiting value of the in-plane correlation length. Accordingly, the homogeneous domains exceed $L_{ab} = (\Phi_0/aH_c)^{1/2} \simeq 2.1 \times 10^{-6}$ cm. The minimum of the dip at

$$t_p(H_c)H_c^{-3/4} = -0.0095\left(\mathrm{T}^{-3/4}\right), \tag{29}$$

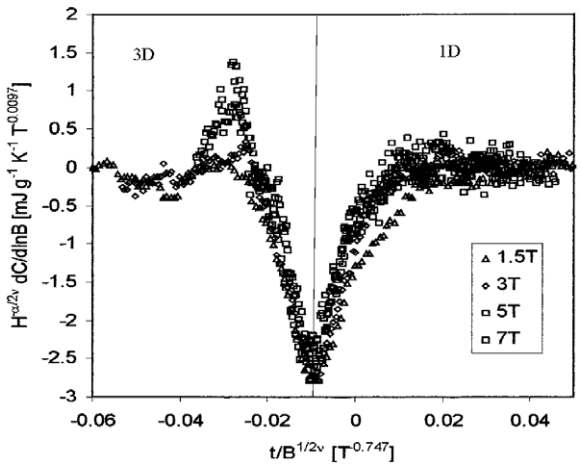


**Figure 6.** Scaling plot $H_c^{1+\alpha/2\nu}\partial(C/T)/\partial H_c$ versus $tH_c^{-1/2\nu}$ for a $DyBa_2Cu_3O_{6.97}$ with $T_c = 91.05$ K, taken from Garfield *et al* [14]. The vertical line indicates the 3D–1D crossover (equation (29)).

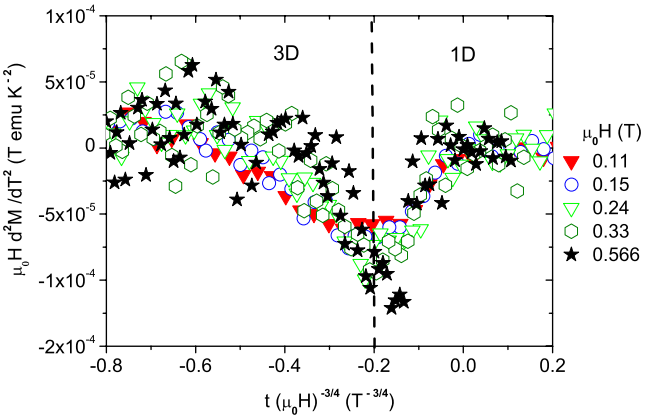


**Figure 7.** Scaling plot $\mu_0 H\, d^2M/dT^2$ versus $t(\mu_0 H)^{-3/4}$ for a $RbOs_2O_6$ powder sample with $T_c = 6.5$ K derived from the magnetization data of Khasanov *et al* [17]. The vertical dashed line is the 1D to 3D crossover line (equation (33)).

fixing the 3D–1D crossover line, yields, with equation (13) for the critical amplitude of the in-plane correlation length, the estimate

$$\xi_{ab0}^{-} \simeq 25\ \text{Å}. \tag{30}$$

The sharp peak in the 3D regime at

$$t_m(H_c)H_c^{-3/4} \simeq -0.028\left(\mathrm{T}^{-3/4}\right), \tag{31}$$

uncovers again the vortex melting line. From the estimates (29) and (31) we obtain

$$\begin{aligned} z_m/z_p &= \left(t_p(H_c)/t_m(H_c)\right)^{2\nu} \simeq 0.24, \\ t_p(H_c)/t_m(H_c) &\simeq 0.34, \end{aligned} \tag{32}$$

in reasonable agreement with the values listed in table 1 for $YBa_2Cu_4O_8$, $NdBa_2Cu_3O_{7-\delta}$, and $YBa_2Cu_3O_{6.97}$. Furthermore, these estimates for the 3D–1D crossover line and the melting line agree well with $t_p(H_c)H_c^{-3/4} = -0.012$ $(\mathrm{T}^{-3/4})$ and $t_m(H_c)H_c^{-3/4} \simeq -0.029$ $(\mathrm{T}^{-3/4})$, derived from the respective peak positions in the total specific heat $C/T$ of an untwinned $YBa_2Cu_3O_{7-x}$ single crystal with $T_c = 91.87$ K, measured by Schilling *et al* [31].

Next we consider the reversible magnetization of the recently discovered superconductor $RbOs_2O_6$ [54]. It is a transition metal (TM) oxide; these are of considerable interest because their properties range from metal–insulator transitions to colossal magnetoresistance and superconductivity. TM oxide compounds with the pyrochlore structure have long been studied and have found many applications [55], but it was not until recently that superconductivity was discovered in one such material, namely, $Cd_2Re_2O_7$ at $T_c \simeq 1$ K [56–58]. Subsequently, superconductivity was also discovered in the pyrochlore oxides $KOs_2O_6$ ($T_c \simeq 9.6$ K) [59], $RbOs_2O_6$ ($T_c \simeq 6.3$ K) [54], and $CsOs_2O_6$ ($T_c \simeq 3.3$ K) [60]. Specific heat [61, 62], magnetization, and muon-spin-rotation ($\mu$SR) studies of the magnetic penetration depth [63, 64], and pressure effect measurements [63] on $RbOs_2O_6$ reveal consistent evidence for mean-field behavior, except close to $T_c$, where thermal fluctuations are observed. Indeed, the analysis of extended measurements of the temperature dependence of the magnetic penetration depth $\lambda$ strongly suggests that $RbOs_2O_6$ falls in the universality class of charged superconductors because charged critical fluctuations were found to dominate the temperature dependence of $\lambda$ near $T_c$ [65]. This differs from the mean-field behavior observed in conventional superconductors and the uncharged (3D $xy$) critical behavior found in nearly optimally doped cuprate superconductors [26, 27, 43, 46], but agrees with the theoretical predictions for charged criticality [66–68] and the charged critical behavior observed in underdoped $YBa_2Cu_3O_{6.59}$ [69]. Noting that in the charged case the magnetic susceptibility scales as $\chi \propto t^{-\nu}$, where $\nu$ adopts the 3D $xy$ value [70] (equation (10)), one expects the scaling form (8) to apply.

In figure 7 we depict the resulting scaling plot for a $RbOs_2O_6$ powder sample with $T_c \simeq 6.5$ K. The vertical dashed line is the 3D–1D crossover line

$$t_p(\mu_0 H)^{-3/4} \simeq -0.2\left(\mathrm{T}^{-3/4}\right), \tag{33}$$

yielding, with equation (12) for the critical amplitude of the correlation length, the estimate

$$\xi_0^{-} \simeq 88\ \text{Å}, \tag{34}$$

in comparison with the mean-field value $\xi(0) \simeq 74$ Å [61, 62]. In the 3D $xy$ universality class, $\xi_0^{-}$ and $\xi_0^{+}$ are related by $\xi_0^{-}/\xi_0^{+} \simeq 2.21$ [49], while charged criticality exhibits inverted 3D $xy$ behavior [71]. Given then the evidence for charged criticality in $RbOs_2O_6$ and the associated critical amplitude of the magnetic penetration depth $\lambda_0 \simeq 1420$ Å [65], we obtain for the Ginzburg–Landau parameter the estimate $\kappa \simeq 1420/(2.21 \times 88) \simeq 7.3$. Accordingly, the resulting effective dimensionless charge [72] $\widetilde{e} = 1/\kappa \simeq 0.14$ is no longer negligible, and is large in comparison with those for extreme type-II superconductors. Furthermore, according to equations (16), (23), (28), (32), and (33) the vortex melting line is expected to occur close to

$$t_m(\mu_0 H)^{-3/4} \simeq -0.63\left(\mathrm{T}^{-3/4}\right), \tag{35}$$

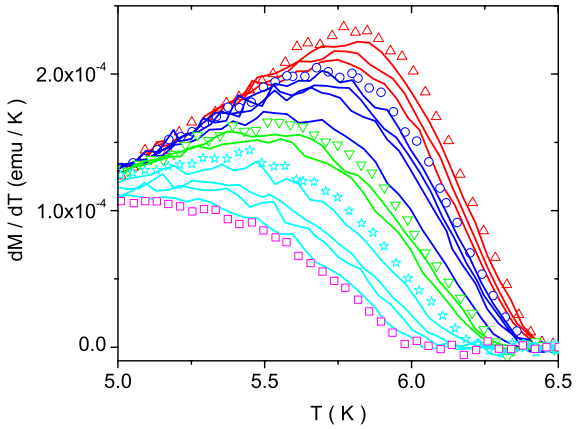


**Figure 8.** $dM/dT$ versus $T$ for a $RbOs_2O_6$ powder sample at various applied magnetic fields, reproduced with permission from Khasanov *et al* [17]. ($\mu_0 H = 0.11$ (△), 0.12, 0.13, 0.14, 0.15 (○), 0.16, 0.17, 0.18, 0.22, 0.24 (▽), 0.26, 0.28, 0.333 (★), 0.366, 0.433, 0.466, and 0.533 T (□)).

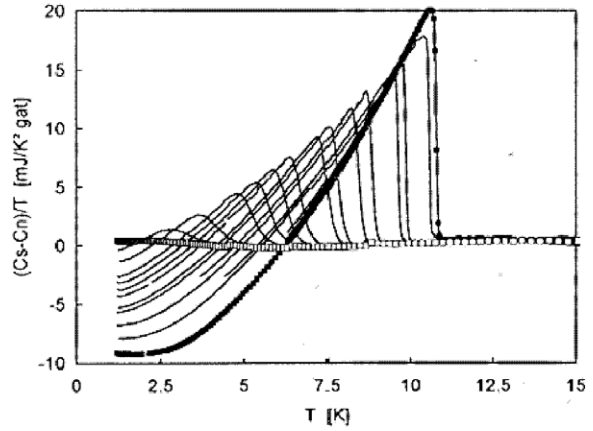


**Figure 9.** $\Delta C/T$ versus $T$ for $Nb_{77}Zr_{23}$ reproduced with permission from Mirmelstein *et al* [18] for various applied magnetic fields (■) 0, (lines) 0.2, 1, 1.2, 2, 2.4, 3, 3.3, 4, 4.4, 4.8, 5.2, 6, 6.6 T (lines), and (□) 7.2 T.

where in figure 7 a peak structure in the 3D regime can be anticipated. Remarkably, despite the comparatively large critical amplitude of the correlation length, the critical regime is accessible. Finally, from $L_{H_c} = (\Phi_0/(aH_c))^{1/2}$, $a \simeq 3.12$ and $\mu_0 H_c = 1.1 \times 10^3$ T, we obtain for the spatial extent of the homogeneous domains in the $RbOs_2O_6$ sample the lower bound $L_{ab} > 1.4 \times 10^{-5}$ cm. In figure 8, showing $dM/dT$ versus $T$ for a $RbOs_2O_6$ powder sample at various applied magnetic fields, we observe that the aforementioned occurrence of an inflection point at $T_p(H)$ is well confirmed.

We have seen that in $YBa_2Cu_4O_8$, $NdBa_2Cu_3O_{7-\delta}$, $YBa_2Cu_3O_{6.97}$, and $DyBa_2Cu_3O_{6.97}$, where for zero magnetic field the occurrence of 3D $xy$ critical behavior is well established [13, 23, 25–27, 39–46], an applied magnetic field does not lead to a continuous phase transition at an upper critical field $H_{c2}$, as predicted by the mean-field approximation. Indeed, the experimental data considered here are fully consistent with a magnetic field induced finite size effect leading to a 3D–1D crossover and a vortex melting line. In table 1 we list the resulting estimates for the universal ratio $z_m/z_p$, $t_p/t_m$, and the critical amplitude of the in-plane correlation length $\xi^-_{ab0}$ below $T_c$.

Since reduced dimensionality enhances thermal fluctuations, one expects that even in conventional type-II superconductors with comparatively large correlation volume the magnetic field induced finite size effect and the associated 3D–1D crossover are at work, although the fluctuation dominated regime may not be accessible in zero magnetic field. To clarify this supposition we analyze in the following the specific heat data for $Nb_{77}Zr_{23}$ [18], $Nb_3Sn$ [19], and $NbSe_2$ [20].

$Nb_{77}Zr_{23}$ is a cubic and isotropic type-II superconductor with $\kappa \simeq 22$. A glance at figure 9 reveals that the effect of the magnetic field on the specific heat jump is initially a shift of its position and a reduction of its height. Since the zero-field anomaly is only 50 mK wide the fluctuation dominated regime is for sufficiently low fields not attained. Nevertheless, we observe that the jump smears out and crosses over to a peak

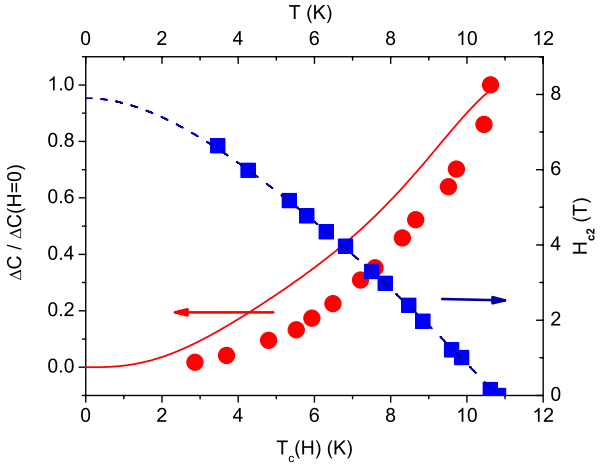


**Figure 10.** $\Delta C/\Delta C(H=0)$ versus $T_c(H)$ (●) and $H_{c2}(T)$ versus $T$ (■) for $Nb_{77}Zr_{22}$. The solid line is obtained from equation (36) and the fitted $H_{c2}(T) = H_{c2}(0)(1-\tilde{t}^2)(1-1.181\tilde{t}^2+1.614\tilde{t}^3-0.712\tilde{t}^4)$ with $H_{c2}(0) = 7.9$ T, $\tilde{t} = T/T_c$, and $T_c = 10.8$ K taken from [18], neglecting the $T$ dependence of the Ginzburg–Landau parameter $\kappa$. The estimates for $H_{c2}(T)$ versus $T$ (■) are derived from figure 9 in the form of the 'transition' mid-points.

which broadens and diminishes with increasing field. In view of this it is not surprising that the mean-field approximation describes the data below 3 T rather well in terms of an upper critical field $H_{c2}$ and an assumed continuous phase transition at $T_c(H)$, estimated from the 'transition' mid-points in figure 9 [18]. To illustrate this point and to uncover the limitations of the mean-field approach, we note that the size of the specific heat jump $\Delta C$ is related to $H_{c2}(T)$ as follows [73]:

$$\Delta C(T_c(H)) \propto \frac{T_c(H)}{2\kappa^2(T_c(H)) - 1} \left(\frac{dH_{c2}}{dT}\right)^2 \Bigg|_{T_c(H)}, \qquad (36)$$

where $\kappa$ is the Ginzburg–Landau parameter. In figure 10 we depict the resulting dependence $\Delta C(T_c(H))/\Delta C(H = 0)$, invoking the $H_{c2}(T)$ taken from Mirmelstein *et al* [18]. Apparently, this approach describes the reduction of the jump reasonably well. Nevertheless, because an applied magnetic

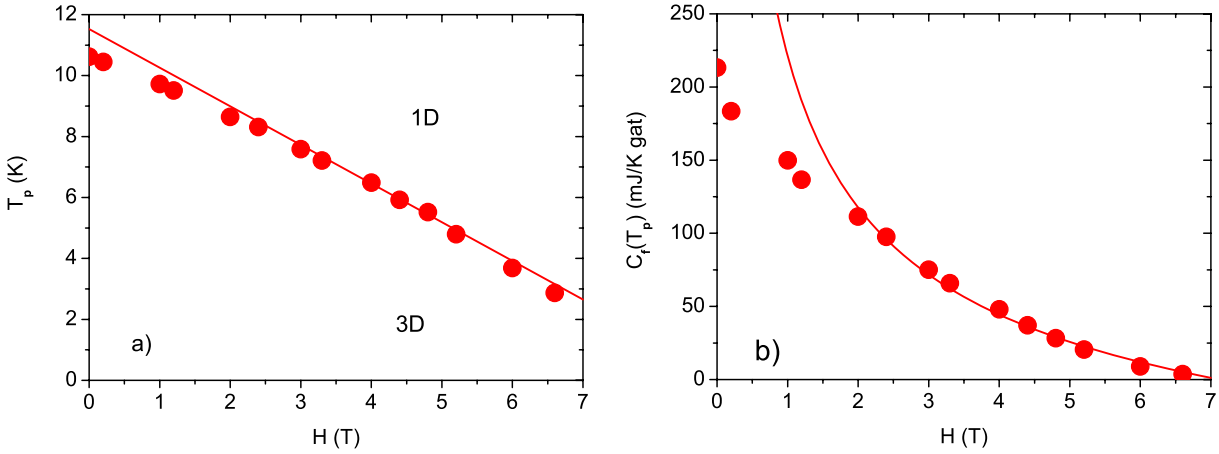


**Figure 11.** (a) 3D–1D crossover line, for $T_p$ versus $H$ for $Nb_{77}Zr_{22}$, derived from the data shown in figure 9. The solid line is equation (37). (b) $C_f(T_p)$ versus $H$ for $Nb_{77}Zr_{23}$ derived from the data shown in figure 9. The solid line is equation (41).

field drives a 3D–1D crossover and, with that, enhances fluctuations, the mean-field approximation is expected to break down in sufficiently high fields. An essential signature of this scenario is the broadening of the specific heat peak, its reduction with increasing field and the field dependence of the peak location $T_p(H)$. From $T_p$ versus $H$ shown in figure 11(a) it is seen that in the regime where the jump broadens substantially ($H > 2$ T), consistency with Gaussian fluctuation behavior,

$$T_p(H) = 11.53 - 1.29H, \tag{37}$$

sets in. Indeed, the linear relationship corresponds to equation (7) with $\nu = 1/2$, the critical exponent of the correlation length for Gaussian fluctuations (equation (11)). This yields for the amplitude of the correlation length the estimate

$$\xi_0^- \simeq 86 \text{ Å}. \tag{38}$$

In addition, figure 9 reveals that the jump broadens and the height of the resulting peak decreases with increasing field. To explore the consistency of this behavior with the magnetic field induced finite size effect, implying enhanced thermal fluctuations due to the 3D–1D crossover, we consider next the magnetic field dependence of the peak height

$$C_f(T_p) = C(T_p) - C_b(T_p), \tag{39}$$

where $C_b(T_p)$ is the temperature dependent background. When the Gaussian scenario holds true, $C_f(T_p)$ scales according to equation (A.11) as

$$C_f(T_p) = \frac{A^-}{\alpha} |x_p|^{-\alpha} f_c^- (x_p) H^{-\alpha/2\nu} + B, \tag{40}$$

with $\alpha = 1/2$ and $\nu = 1/2$, characteristic for Gaussian fluctuations (equation (11)). From figure 11(b), showing $C_f(T_p)$ versus $H$, it is seen that

$$C_f(T_p) = -132.44 + 353.64H^{-1/2}, \tag{41}$$

with $C_f(T_p)$ in mJ K$^{-1}$ (g atom)$^{-1}$ and $H$ in T, describes the experimental data in the high field regime rather well. To substantiate the consistency with Gaussian thermal fluctuations further, we note that data taken in sufficiently high fields should collapse onto a single curve when plotted as $H^{1/2}(C_f - B)$ versus $t/H$. In figure 12 we observe remarkable consistency with this scaling behavior, characteristic for a magnetic field induced finite size effect associated with Gaussian fluctuations (equation (11)), enhanced by the 3D–1D crossover. This crossover line, $t_p/H = -0.11$ (T$^{-1}$), yields for the critical amplitude of the correlation length the estimate $\xi_0^- \simeq 85$ Å, in agreement with equation (38).

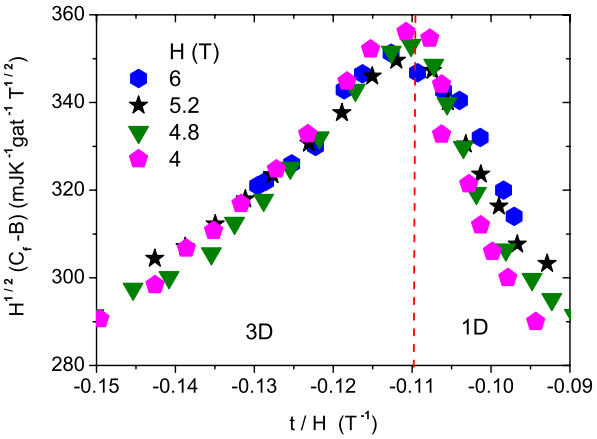


**Figure 12.** Scaling plot $H^{1/2}C_f$ versus $t/H$ for $Nb_{77}Zr_{23}$ derived from the data shown in figure 9 with $B = -132.44$ (mJ K$^{-1}$ (g atom)$^{-1}$; equation (41)). The vertical dashed line marks $t_p/H = -0.11$ (T$^{-1}$), the 3D–1D crossover line.

While the utilization of high $T_c$ cuprates made considerable progress in recent years, triniobium stannite ($Nb_3Sn$) is still one of the most important materials for the practical application of superconductivity more than fifty years after its discovery [74], most notably as superconducting wires in high field magnets. $Nb_3Sn$ belongs to a class of $A_3B$ binary intermetallic compounds with the A15 or $\beta$-tungsten structure, where those based on Nb give rise to a subclass that includes $Nb_3Ge_2$ [75], having the highest $T_c$ ($\simeq$23 K) for more than thirty years, and therefore it was once a subject of intensive

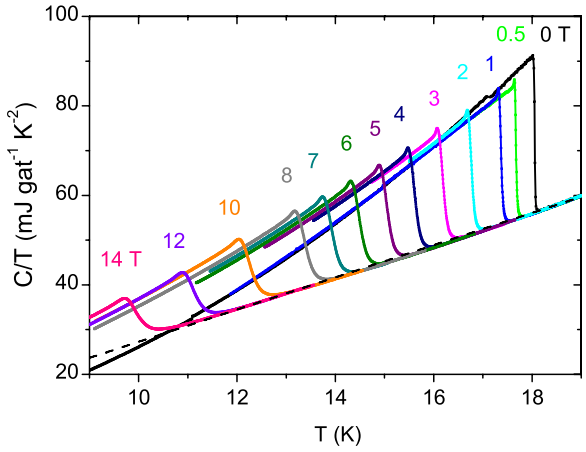


**Figure 13.** Total specific heat of a single crystal of $Nb_3Sn$ in fields from 0 to 14 T measured by an ac technique, reproduced with permission from Lortz *et al* [19]. The dashed line is $C_b/T = -8.72 + 3.6T$ (mJ (g atom)$^{-1}$ K$^{-2}$), taken as the temperature dependent background.

study, until the 1970s [76]. Surprisingly, it seems that the fundamental superconducting properties of $Nb_3Sn$ are not fully understood. In figure 13 we depict the total specific heat of a $Nb_3Sn$ single crystal measured by Lortz *et al* [19] in fields from 0 to 14 T. In zero field, consistency with the typical mean-field jump is observed and there appears to be no signature of fluctuations as the superconducting phase is entered from the normal state. However, with increasing magnetic field the jump broadens and the height of the resulting peak decreases. To explore the consistency of this behavior with the magnetic field induced finite size effect, we explore the scaling of the peak position $T_p(H)$ and of the fluctuation contribution $C_f(T_p)$ to the specific heat. From figure 14(a) it is seen that the linear relationship

$$T_p(H) = 17.86\,(1 - 0.033H)\,(\mathrm{K}), \qquad t_p/H = -0.033\ \left(\mathrm{T}^{-1}\right), \tag{42}$$

for the 3D–1D crossover line describes the data rather well. This uncovers, with equation (7), Gaussian fluctuations (equation (11)) with

$$\xi_0^- \simeq 46\ \text{Å}, \tag{43}$$

for the critical amplitude of the correlation length. When this Gaussian scenario holds true, $C_f(T_p)$ should then scale according to equation (11). From figure 14(b), showing $C_f(T_p)$ versus $H$, it is seen that

$$C_f(T_p) = -173.3 + 1115H^{-1/2}\ (\mathrm{mJ\ K^{-1}\ (g\ atom)^{-1}}), \tag{44}$$

describes the experimental data for sufficiently high fields rather well and conforms with a magnetic field induced finite size effect scenario driven by Gaussian fluctuations.

Furthermore, the more detailed plot of the specific heat coefficient depicted in figure 15 uncovers in the low field regime and below the mean-field jump a weak peak. This anomaly, marked by arrows, was traced back to the vortex melting transition [19] and conforms with enhancement of thermal fluctuations with increasing field strength. The resulting melting line, consistent with

$$T_m(H) = 18\,(1 - 0.036H)\,, \qquad t_m/H = -0.036\,\left(\mathrm{T}^{-1}\right), \tag{45}$$

is shown in figure 16 and reveals again consistency with Gaussian fluctuations. For comparison we included the 3D–1D crossover line, disclosing that the vortex melting transition occurs in the 3D regime. From equations (42) and (45) we obtain in the Gaussian case with $z_m/z_p = (t_p/t_m)^{2\nu}$ (equation (32)) for the universal ratio the estimate

$$t_p(H)/t_m(H) = z_m/z_p \simeq 0.92, \tag{46}$$

which differs substantially from the 3D $xy$ value $t_p(H_c)/t_m(H_c) \simeq 0.32$ (equations (23), (28) and (32)).

So far we considered either anisotropic superconductors in magnetic fields applied along the $c$-axis or isotropic materials. A suitable anisotropic type-II superconductor for which the effects of the magnetic field on the specific heat, for fields applied parallel and perpendicular to the layers, have been

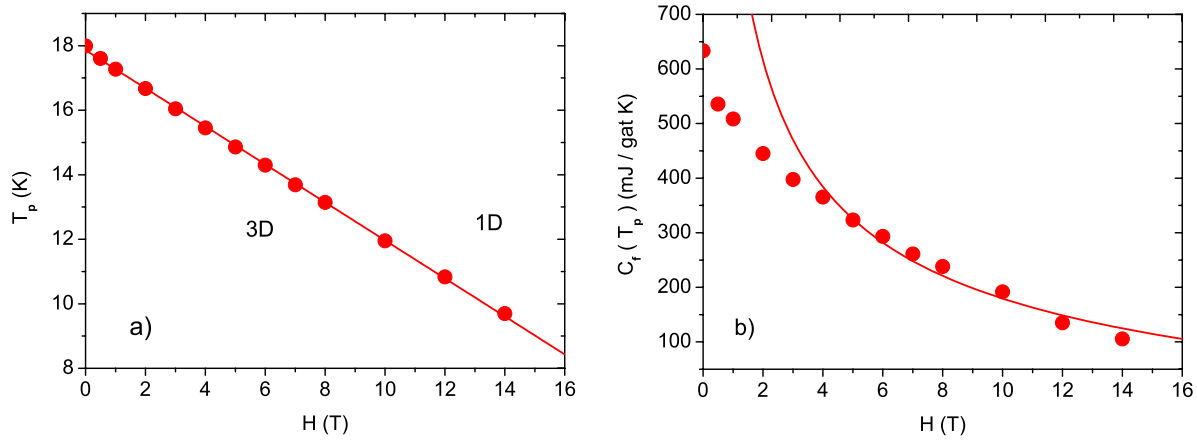


**Figure 14.** (a) 3D–1D crossover line, $T_p$ versus $H$, for $Nb_3Sn$ deduced from the specific heat data shown in figure 13. The solid line is equation (42). (b) $C_f(T_p)$ versus $H$ for $Nb_3Sn$ derived from the data shown in figure 13. The solid line is equation (44) with $C_b(T_p)/T_p = -8.72 + 3.6T_p$ (mJ (g atom)$^{-1}$ K$^{-2}$), indicated in figure 13.

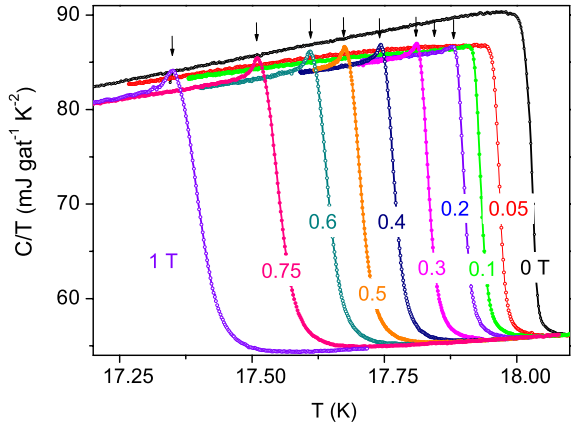


**Figure 15.** Total specific heat of a single crystal of $Nb_3Sn$ in fields from 0 to 1 T, reproduced with permission from Lortz *et al* [19]. The arrows mark the location of the vortex melting transition.

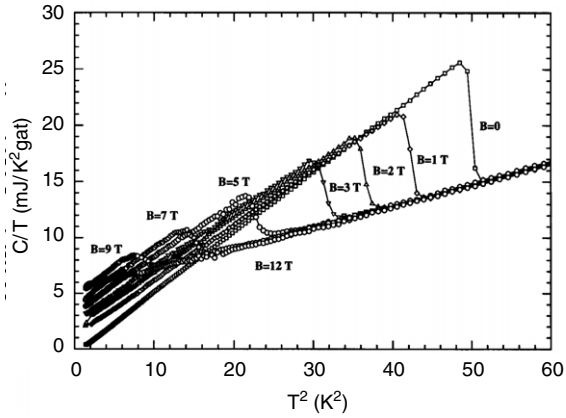


**Figure 17.** Specific heat of a $NbSe_2$ single crystal in various magnetic fields applied parallel to the layers, reproduced with permission from Sanchez *et al* [20].

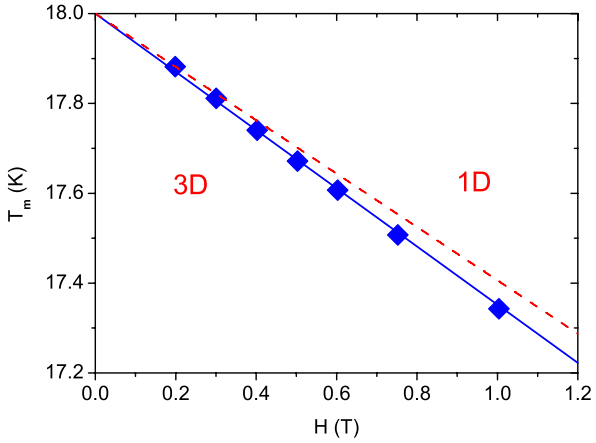


**Figure 16.** Vortex melting line, $T_m$ versus $H$, for $Nb_3Sn$ derived from the location of the marked anomalies in figure 15. The solid line is the melting line (equation (45)) and the dashed one the 3D–1D crossover line (equation (42)).

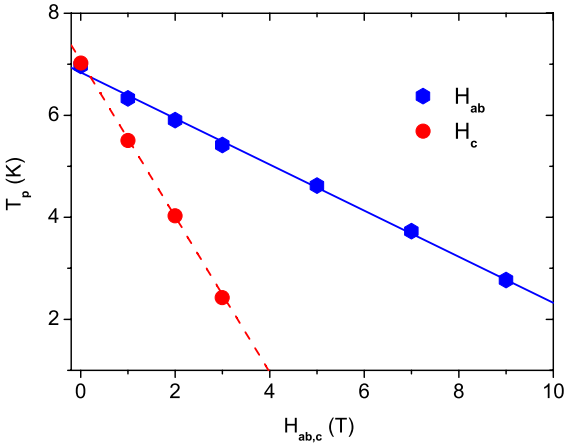


**Figure 18.** 3D–1D crossover lines, $T_p$ versus $H_{ab,c}$, for $NbSe_2$ deduced from the specific heat data of Sanchez *et al* [20]. The solid line is equation (47), the 3D–1D crossover line for fields applied parallel to the *ab*-plane, and the dashed one is equation (48), the dimensional crossover line for fields applied parallel to the *c*-axis.

studied in some detail is $NbSe_2$ [20]. Moreover, the relevance of fluctuations was established already some time ago by Frindt [77] in terms of the dependence of $T_c$ on the crystal thickness, reduced below six $NbSe_2$ layers. In figure 17 we reproduce the specific heat data of Sanchez *et al* [20] for a $NbSe_2$ single crystal in various magnetic fields applied parallel to the layers. Like for $Nb_{77}Zr_{23}$ (figure 9) and $Nb_3Sn$ (figure 13) the jump broadens and its height decreases with increasing magnetic field. The same behavior was observed for fields applied perpendicular to the layers [20]. In figure 18 we depict $T_p$ versus $H_{ab}$ and $H_c$ for $NbSe_2$ derived from figure 17 and the data of Sanchez *et al* [20]. The solid and dashed lines are

$$T_p\,(H_{ab}) = 6.84\,(1 - 0.066 H_{ab})\ \ (\mathrm{K}), \tag{47}$$

$$T_p(H_c) = 7.07\,(1 - 0.216 H_{ab})\ \ (\mathrm{K}), \tag{48}$$

revealing consistency with a 3D–1D crossover line associated with Gaussian fluctuations (equation (11)). Invoking equation (1) we obtain for the critical amplitudes of the correlation lengths and the anisotropy $\gamma$ the estimates

$$\xi^-_{ab0} \simeq 120\ \text{Å}, \qquad \left(\xi^-_{ab0}\xi^-_{c0}\right)^{1/2} = 66\ \text{Å}, \tag{49}$$

and

$$\xi^-_{c0} \simeq 36\ \text{Å}, \qquad \gamma = \xi^-_{ab0}/\xi^-_{c0} \simeq 1.8, \tag{50}$$

to be compared to the previous estimate, $\gamma \simeq 2.4$ [78], for the anisotropy. When this crossover line stems from Gaussian fluctuations the extension of equation (A.11) to anisotropic systems implies that the peak height $C_f(T_p(H_{ab,c}))$ scales as

$$c_f(T_p(H_c)) = \frac{A^-}{\alpha} f_c^-\left(x_{pc}\right)\left(\frac{\left(\xi^-_{ab0}\right)^2 a H_c}{\Phi_0}\right)^{-\alpha/2\nu} + B_c, \tag{51}$$

for fields applied parallel to the *c*-axis where

$$x_{pc} = \frac{t_p}{H_c^{1/2\nu}} = \left(\frac{\left(\xi^-_{ab0}\right)^2 a}{\Phi_0}\right)^{1/2\nu} \tag{52}$$

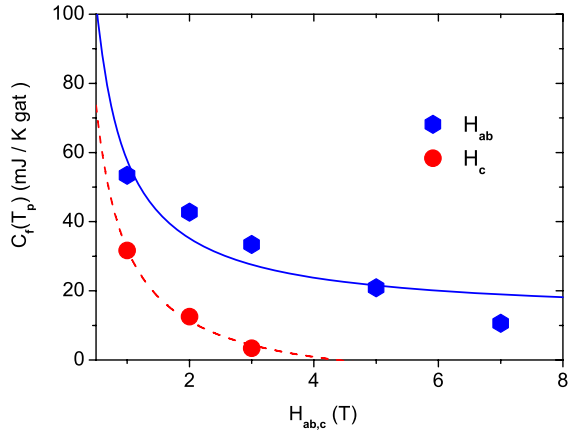


**Figure 19.** $C_f(T_p)$ versus $H_{ab,c}$ for $NbSe_2$, derived from the specific heat data of Sanchez *et al* [20]. The solid line is equation (55) with $C_b(T_p(H_{ab}))/T_p = 4.95 + 0.196T_p^2$ mJ K$^{-2}$ (g atom)$^{-1}$ and the dashed one equation (56) with $C_b(T_p(H_c))/T_p(H_c) = 5.06 + 0.193T_p^2$ mJ K$^{-2}$ (g atom)$^{-1}$ taken as the temperature dependent background.

and for fields applied in the $ab$-plane

$$c_f\left(T_p\left(H_{ab}\right)\right) = \frac{A^-}{\alpha} f_c^-\left(x_{pab}\right)\left(\frac{\xi_{ab0}^-\xi_{c0}^- a H_{ab}}{\Phi_0}\right)^{-\alpha/2\nu} + B_{ab}, \tag{53}$$

where

$$x_{pab} = \frac{t_p}{H_c^{1/2\nu}} = \left(\frac{\xi_{ab0}^-\xi_{c0}^- a}{\Phi_0}\right)^{1/2\nu}, \tag{54}$$

with $\alpha = 1/2$ and $\nu = 1/2$ for Gaussian fluctuations (equation (11)). In figure 19 we show $C_f(T_p(H_{ab,c}))$ versus $H_{ab,c}$ derived from the data of Sanchez *et al* [20]. For comparison we included the fits

$$C_f\left(T_p\left(H_{ab}\right)\right) = -9.13 + 66.45H_{ab}^{-1/2}\ (\text{mJ K}^{-1}\ (\text{g atom})^{-1}), \tag{55}$$

$$C_f\left(T_p(H_c)\right) = -34.97 + 66.8H_c^{-1/2}\ (\text{mJ K}^{-1}\ (\text{g atom})^{-1}), \tag{56}$$

which describe the sparse data reasonably well and conform with the 3D–1D crossover arising from the magnetic field induced finite size effect tuned by Gaussian fluctuations. In addition, the ratio $66.45/66.8 \simeq \xi_{ab0}^-/\xi_{c0}^- \simeq \gamma \simeq 1$, provides an independent estimate of the anisotropy. While the rather limited resolution of the specific heat data for $NbSe_2$ (figure 17) does not reveal any signature of the thermodynamic vortex melting transition, mode locking and dc transport measurements uncovered this transition over a wide magnetic field and temperature range [79]. Accordingly, the universal ratio between the 3D–1D crossover and vortex melting line (equation (46)) is expected to apply.

The characteristic features of the magnetic field induced finite size effect on the specific heat, broadening of the peak and the reduction of its height with increasing field, have also been observed for $ZrB_{12}$ [80] and $\kappa$-(BEDT-TTF)$_2$Cu(NCS)$_2$ [81]. In contrast to the systems considered so far, these materials exhibit a richer response to an applied magnetic field. While in most type-II superconductors the orbital pair-breaking mechanism dominates, this is no longer the case for $\kappa$-(BEDT-TTF)$_2$Cu(NCS)$_2$. In parallel fields above 21 T the Pauli-paramagnetic pair-breaking effects appear and there is evidence for the Fulde–Ferrel–Larkin–Ovchinnikov phase [82, 83]. Furthermore, clean $ZrB_{12}$ with $T_c \simeq 6$ K is a superconductor whose Ginzburg–Landau parameter $\kappa \simeq 0.65$ is close to the border value $2^{-1/2} \simeq 0.7$. Since $\kappa$ varies with temperature the material crosses over from the type-I to the type-II case as the temperature is lowered.

## 4. Summary and conclusions

We have seen that measurements of thermodynamic properties have evolved into a major experimental tool in the quest for an understanding of type-II superconductors. Noting that the influence of magnetic fields on the superconducting state is of great technological relevance, this issue is not just of fundamental interest. Nevertheless, the effects of thermal fluctuations were not fully identified over several decades. Particularly for classical superconductors, including $Nb_{77}Zr_{23}$, $Nb_3Sn$ and $NbSe_2$, interpretations based on the standard mean-field approximation were considered to be satisfactory. By contrast, our analysis of the specific heat data uncovered for sufficiently high fields remarkable consistency with the magnetic field induced finite size effect, giving rise to a 3D–1D crossover which enhances thermal fluctuations. While in $YBa_2Cu_4O_8$, $NdBa_2Cu_3O_{7-\delta}$, $YBa_2Cu_3O_{7-\delta}$, and $DyBa_2Cu_3O_{7-\delta}$ 3D $xy$ fluctuations, and in $RbOs_2O_6$ inverted 3D $xy$ thermal fluctuations were shown to drive this crossover, the specific heat data for the conventional type-II superconductors $Nb_{77}Zr_{23}$, $Nb_3Sn$ and $NbSe_2$ point to Gaussian fluctuations. In any case, whenever this crossover occurs there is no continuous phase transition in the $H$–$T$-plane along an $H_{c2}(T)$-line, as predicted by the mean-field treatment. Instead there is the 3D–1D crossover line $H_{pi}(T) = (\Phi_0/(a\xi_{j0}^-\xi_{k0}^-))(1 - T/T_c)^{1/2\nu}$ with $i \neq j \neq k$ and $\xi_{i0,j0,k0}^-$ denoting the critical amplitude of the correlation length below $T_c$ with critical exponent $\nu$. Accordingly, below $T_c$ and above $H_{pi}(T)$ superconductivity is confined to cylinders with diameter $L_{H_i} \propto H_i^{-1/2}$, whereupon the system becomes 1D. However, 1D systems with short range interactions do not undergo a continuous phase transition at finite temperature [68] and, with that, there is no continuous phase transition in the $H$–$T$-plane above the 3D–1D crossover line. Furthermore, we have shown that the thermodynamic vortex melting transition occurs in the 3D regime. While in $YBa_2Cu_4O_8$, $NdBa_2Cu_3O_{7-\delta}$, $YBa_2Cu_3O_{7-\delta}$, and $DyBa_2Cu_3O_{7-\delta}$ it is driven by 3D $xy$ thermal fluctuations, the specific heat data for the conventional type-II superconductors $Nb_{77}Zr_{23}$, $Nb_3Sn$ and $NbSe_2$ point to Gaussian fluctuations. In any case, because the vortex melting transition and the 3D–1D crossover occur at universal values of the scaling variable $z$, the ratio $z_m/z_p = (t_p(H_c)/t_m(H_c))^{2\nu}$ should be universal as well. Our analysis revealed $z_m/z_p = (t_p(H_c)/t_m(H_c))^{2\nu} \simeq 0.23$ (equations (23), (28) and (32)), when 3D $xy$ fluctuations dominate, and $z_m/z_p = t_p(H)/t_m(H) \simeq 0.92$ (equation (46)) in the Gaussian case. Thus it appears that thermal fluctuations, enhanced by the 3D to 1D crossover, are important not only

for high temperature superconductors but also for conventional type-II superconductors with comparatively large correlation volume. This observation opens up a window onto the universal properties mediated by thermal fluctuations and allows us to probe the thermodynamically relevant spatial extent of the homogeneous domains. From this perspective, more extended high resolution specific heat and reversible magnetization measurements on type-II superconductors and their analyses along the lines outlined here will certainly be necessary to unravel the details of the universal properties associated with the 3D–1D crossover and the vortex melting transition in type-II superconductors.

## Acknowledgments

Over the years, we have benefited from numerous scientific discussions on this topic with H Keller, R Khasanov, R Lortz, C Meingast, K A Müller, J Roos, J M Singer, and S Weyeneth. Moreover, the author is grateful to R Khasanov, and R Lortz for providing experimental data.

## Appendix

When in a type-II superconductor thermal fluctuations dominate and the coupling to the charge is negligible, the free energy per unit volume adopts in the presence of a magnetic field $H_c$ applied parallel to the $c$-axis the scaling form (3). This leads for the magnetization per unit volume $m = M/V = -\partial f_s/\partial H_c$ the scaling expression [13, 26, 27, 44]

$$\frac{m}{TH^{1/2}} = -\frac{Q^{\pm}k_B\xi_{ab}}{\Phi_0^{3/2}\xi_c}F^{\pm}(z), \qquad F^{\pm}(z) = z^{-1/2}\frac{dG^{\pm}}{dz},$$
$$z = x^{-1/2\nu} = \frac{\left(\xi_{ab0}^{\pm}\right)^2|t|^{-2\nu}H_c}{\Phi_0}. \tag{A.1}$$

$Q^{\pm}$ is a universal constant and $G^{\pm}(z)$ a universal scaling function of its argument, with $G^{\pm}(z=0)=1$. $\gamma = \xi_{ab}/\xi_c$ denotes the anisotropy, $\xi_{ab}$ the zero-field in-plane correlation length and $H_c$ the magnetic field applied along the $c$-axis. In terms of the variable $x$ the scaling form (1) is similar to Prange's [51] result for Gaussian fluctuations. Approaching $T_c$ the in-plane correlation length diverges as

$$\xi_{ab} = \xi_{ab0}^{\pm}|t|^{-\nu}, \qquad t = T/T_c - 1, \qquad \pm = \mathrm{sgn}(t). \tag{A.2}$$

Supposing that 3D $xy$ fluctuations dominate, the critical exponents are given by [48, 49]

$$\nu \simeq 0.671 \simeq 2/3, \qquad \alpha = 2\nu - 3 \simeq -0.013, \tag{A.3}$$

and there are the universal critical amplitude relations [13, 26, 27, 44, 48, 49]

$$\frac{\xi_{ab0}^-}{\xi_{ab0}^+} = \frac{\xi_{c0}^-}{\xi_{c0}^+} \simeq 2.21, \qquad \frac{Q^-}{Q^+} \simeq 11.5, \qquad \frac{A^+}{A^-} = 1.07, \tag{A.4}$$

and

$$A^-\xi_{a0}^-\xi_{b0}^-\xi_{c0}^- \simeq A^-\left(\xi_{ab0}^-\right)^2\xi_{c0}^- = \frac{A^-(\xi_{ab0}^-)^3}{\gamma}$$
$$= \left(R^-\right)^3, \qquad R^- \simeq 0.815, \tag{A.5}$$

where $A^{\pm}$ is the critical amplitude of the specific heat singularity, defined as

$$c = \frac{C}{Vk_B} = \frac{A^{\pm}}{\alpha}|t|^{-\alpha} + B, \tag{A.6}$$

where $B$ denotes the background. Furthermore, in the 3D $xy$ universality class, $T_c$, $\xi_{c0}^-$ and the critical amplitude of the in-plane penetration depth $\lambda_{ab0}$ are not independent but related by the universal relation [13, 26, 27, 44, 49]:

$$k_BT_c = \frac{\Phi_0^2}{16\pi^3}\frac{\xi_{c0}^-}{\lambda_{ab0}^2} = \frac{\Phi_0^2}{16\pi^3}\frac{\xi_{ab0}^-}{\gamma\lambda_{ab0}^2}. \tag{A.7}$$

From this universal relation it follows naturally that the isotope and pressure effects on the transition temperature, the correlation lengths, the anisotropy and the magnetic penetration depths are not independent [84, 85]. Furthermore, the existence of the magnetization at $T_c$, of the penetration depth below $T_c$ and of the magnetic susceptibility above $T_c$ imply the following asymptotic forms of the scaling function [13, 26, 27, 44]:

$$Q^{\pm}\left.\frac{1}{\sqrt{z}}\frac{dG^{\pm}}{dz}\right|_{z\to\infty} = Q^{\pm}c_{\infty}^{\pm},$$
$$Q^-\left.\frac{dG^-}{dz}\right|_{z\to 0} = Q^-c_0^-\left(\ln z + c_1\right), \tag{A.8}$$
$$Q^+\left.\frac{1}{z}\frac{dG^+}{dz}\right|_{z\to 0} = Q^+c_0^+,$$

with the universal coefficients

$$Q^-c_0^- \simeq -0.7, \qquad Q^+c_0^+ \simeq 0.9,$$
$$Q^{\pm}c_{\infty}^{\pm} \simeq 0.5, \qquad c_1 \simeq 1.76. \tag{A.9}$$

To relate the magnetization to the peak structure in the specific heat we invoke Maxwell's relation

$$\left.\frac{\partial(C/T)}{\partial H_c}\right|_T = \left.\frac{\partial^2 M}{\partial T^2}\right|_{H_c}, \tag{A.10}$$

uncovering the melting transition in the form of a singularity, while the magnetic field induced finite size effect leads to a dip. These features differ drastically from the nearly smooth behavior of the magnetization. Combining with the scaling form of the specific heat (equation (A.6)), extended to the presence of a magnetic field, we have

$$c = \frac{A^-}{\alpha}|t|^{-\alpha}f^{\pm}(x), \qquad x = \frac{t}{H^{1/2\nu}}, \tag{A.11}$$

where

$$f_c^-(x) = \begin{matrix} 1 & : x \to -\infty \\ f_0^-|x|^{\alpha} & : x \to 0^- \end{matrix}\Bigg\}. \tag{A.12}$$

This yields the scaling form

$$T H_c^{1+\alpha/2\nu} \frac{\partial (c/T)}{\partial H_c} = -\frac{k_B A^-}{2\alpha\nu} x^{1-\alpha} \frac{\partial f}{\partial x} = T H_c^{1+\alpha/2\nu} \frac{\partial^2 m}{\partial T^2}. \tag{A.13}$$

According to this, data plotted as $T H_c^{1+\alpha/2\nu} \partial (c/T)/\partial H_c$ or $T H_c^{1+\alpha/2\nu} \partial^2 m/\partial T^2$ versus $x = t H^{-1/2\nu}$ should collapse onto a single curve as long as the magnetic field induced finite size effect sets the limiting length ($L_{H_c} = (\Phi_0/aH_c)^{1/2} < L_{ab}$). At $T_c$ equation (A.13) reduces to

$$T_c H_c^{1+\alpha/2\nu} \frac{\partial (c/T)}{\partial H_c} = -\frac{k_B A^- f_0^-}{2\nu} = T_c H_c^{1+\alpha/2\nu} \frac{\partial^2 m}{\partial T^2}. \tag{A.14}$$

The scaling form (A.13) can also be derived from equation (A.1) rewritten in the form

$$m = -\frac{Q^- k_B \gamma}{\Phi_0^{3/2}} T H_c^{1/2} f_m(x), \tag{A.15}$$

yielding

$$\frac{\partial m}{\partial T} = -\frac{Q^- k_B \gamma}{\Phi_0^{3/2}} H_c^{1/2} \left( f_m(x) + \frac{T}{T_c} H_c^{-1/2\nu} \frac{\partial f_m(x)}{\partial x} \right), \tag{A.16}$$

and

$$T_c H_c^{-(\nu-2)/2\nu} \frac{\partial^2 m}{\partial T^2} = -\frac{Q^- k_B \gamma}{\Phi_0^{3/2}} \left( 2 \frac{\partial f_m(x)}{\partial x} H_c + \frac{T}{T_c} \frac{\partial^2 f_m(x)}{\partial x^2} \right). \tag{A.17}$$

Noting that

$$-(\nu - 2)/2\nu = (1 + \alpha/2\nu), \tag{A.18}$$

it is readily seen that close to $T_c$ and at low magnetic fields the scaling forms (A.13) and (A.17) agree.

In this context it is instructive to sketch the predictions of the approximation where Gaussian fluctuations are taken into account while the magnetic field induced finite size effect is neglected. In this case the magnetization adopts the scaling form [27, 51]

$$\frac{m}{T H^{1/2}} = -\frac{2\pi^{1/2} k_B}{\Phi_0^{3/2}} \widetilde{f}(\widetilde{x}), \tag{A.19}$$

where

$$\widetilde{x} = \frac{\Phi_0}{4\pi \xi_0^2 H} t. \tag{A.20}$$

Close to $\widetilde{x} = -0.5$ the scaling function adopts the form $\widetilde{f}(\widetilde{x}) = 1/(4(\widetilde{x}+0.5)^{1/2})$. The resulting singularity suggests a continuous phase transition at the so-called upper critical field $H_{c2}(T) = \Phi_0/(2\pi\xi_0^2)|t|$ and implies a divergence of $\partial^2 m/\mathrm{d}T^2$ at $T_{c2}(H)$. However, taking the magnetic field induced finite size effect into account, the growth of the correlation length $\xi$ is limited by $L = (\Phi_0/(aH))^{1/2}$ and the singularity is smeared out in the form of a dip.

Furthermore, from equation (A.11) we obtain for $\mathrm{d}c/\mathrm{d}T$ the scaling form

$$\frac{\mathrm{d}c}{\mathrm{d}T} = \frac{A^-}{T_c} H_c^{-(1+\alpha)/2\nu} \left( x^{-(1+\alpha)/2\nu} f(x) - \alpha x^{-\alpha} \frac{\mathrm{d}f}{\mathrm{d}x} \right), \tag{A.21}$$

whereby the data $\mathrm{d}c/\mathrm{d}T$ for different fields should collapse onto a single curve when plotted as $H_c^{(1+\alpha)/2\nu} T_c \, \mathrm{d}c/\mathrm{d}T$ versus $t H_c^{-1/2\nu}$ as long as $L_{H_c} = (\Phi_0/aH_c)^{1/2} < L_{ab}$. To explore the structure of this plot we consider again the Gaussian approximation. In this case the free energy density (equation (3)) adopts the form [27, 51]

$$f_s = -\frac{k_B T}{6\pi\xi^3} \widetilde{G}(\widetilde{z}), \qquad \widetilde{z} = \frac{4\pi\xi_0^2 H}{\Phi_0} = \frac{1}{\widetilde{x}}, \tag{A.22}$$

Close to $\widetilde{z} = -2$ the scaling function is given by $\widetilde{G}(z) = -(1 + \widetilde{z}/4)(\widetilde{z} - 2) + \text{const}$. The resulting singularity in the specific heat, $c = -T\partial f_s^2/\partial T^2$, suggests again a continuous phase transition at the so-called upper critical field $H_{c2}(T) = \Phi_0/(2\pi\xi_0^2)|t|$ and implies a divergence of $\mathrm{d}c/\mathrm{d}T$ at $T_{c2}(H)$. However, taking the magnetic field induced finite size effect into account, the growth of the correlation length $\xi$ is limited by $L = (\Phi_0/(aH))^{1/2}$ and the singularity is smeared out in the form of a dip.

## References


[1] Ginzburg V L and Landau L D 1950 *Zh. Eksp. Teor. Fiz.* **20** 1064
[2] Abrikosov A A 1957 *Zh. Eksp. Teor. Fiz.* **32** 1442
Abrikosov A A 1957 *Sov. Phys.—JETP* **5** 1174 (Engl. Transl.)
[3] Blatter G *et al* 1994 *Rev. Mod. Phys.* **66** 1125
[4] Nattermann T and Scheidl S 2000 *Adv. Phys.* **49** 607
[5] Dietel J and Kleinert H 2006 arXiv:cond-mat/0612042v2
[6] Lee P A and Shenoy S R 1972 *Phys. Rev. Lett.* **28** 1025
[7] Thouless D J 1975 *Phys. Rev. Lett.* **34** 946
[8] Brezin E, Fujita A and Hikami S 1990 *Phys. Rev. Lett.* **65** 1949
[9] Hikami S and Fujita S 1990 *Phys. Rev.* B **41** 6379
[10] Weyeneth S, Schneider T, Bukowski Z, Karpinski J and Keller H 2008 *J. Phys.: Condens. Matter* **20** 345210
[11] Plackowski T, Wang Y, Lortz R, Junod A and Wolf Th 2005 *J. Phys.: Condens. Matter* **17** 6871
[12] Roulin M, Junod A and Walker E 1998 *Physica* C **296** 137
[13] Schneider T 2007 *Phys. Rev.* B **75** 174517
[14] Garfield N J, Howson M A, Yang G and Abell S 1999 *Physica* C **321** 1
[15] Liang R, Bonn D A and Hardy W N 1996 *Phys. Rev. Lett.* **76** 835
[16] Cooper J R, Loram J W, Johnson D J, Hodby J W and Changkang C 1997 *Phys. Rev. Lett.* **79** 1730
[17] Khasanov R *et al* 2005 unpublished
[18] Mirmelstein M, Junod A, Walker E, Revaz B, Genoud Y Y and Triscone G 1997 *J. Supercond.* **10** 527
[19] Lortz R, Lin F, Musolino N, Wang Y, Junod A, Rosenstein B and Toyota N 2006 *Phys. Rev.* B **74** 104502
[20] Sanchez D, Junod A, Muller J, Berger H and Lévy F 1995 *Physica* B **204** 167
[21] Farrant S P and Gough C E 1975 *Phys. Rev. Lett.* **34** 943
[22] Fisher M E 1971 *Critical Phenomena, Proc. 1970 Int. School of Physics Enrico Fermi, Course 51* ed M S Green (New York: Academic)
[23] Schneider T 2004 *J. Supercond.* **17** 41
[24] Haussmann R 1999 *Phys. Rev.* B **60** 12373
[25] Lortz R, Meingast C, Rykov A I and Tajima S 2003 *Phys. Rev. Lett.* **91** 207001
[26] Schneider T 2004 *The Physics of Superconductors* ed K Bennemann and J B Ketterson (Berlin: Springer) p 111
[27] Schneider T and Singer J M 2000 *Phase Transition Approach To High Temperature Superconductivity* (London: Imperial College Press)

[28] Lawrie I D 1997 *Phys. Rev. Lett.* **79** 131
[29] Crabtree G W and Nelson D R 1997 *Phys. Today* **4** 38–45
[30] Welp U, Fendrich J A, Kwok W K, Crabtree G W and Veal B W 1996 *Phys. Rev. Lett.* **76** 4809
[31] Schilling A *et al* 1997 *Phys. Rev. Lett.* **78** 4833
[32] Safar H, Gammel P L, Huse D A and Bishop D J 1993 *Phys. Rev. Lett.* **70** 3800
[33] Kwok W K, Fendrich J, Fleshler S, Welp U, Downey J and Crabtree G W 1994 *Phys. Rev. Lett.* **72** 1092
[34] Bouquet F *et al* 2001 *Nature* **411** 448
[35] Cardy J L 1998 *Finite-Size Scaling* (Amsterdam: North-Holland)
[36] Privman V 1990 *Finite Size Scaling and Numerical Simulations of Statistical Systems* (New Jersey: World Scientific)
[37] Nho K and Manousakis E 2001 *Phys. Rev.* B **64** 144513
[38] van Hove L 1950 *Physica* **16** 137
[39] Schneider T and Ariosa D 1992 *Z. Phys.* B **89** 267
[40] Schneider T and Keller H 1993 *Int. J. Mod. Phys.* B **8** 487
[41] Overend N, Howson M A and Lawrie I D 1994 *Phys. Rev. Lett.* **72** 3238
[42] Hubbard M A, Salamon M B and Veal B W 1996 *Physica* C **259** 309
[43] Kamal S, Liang R, Hosseini A, Bonn D A and Hardy W N 1998 *Phys. Rev.* B **58** 8933
[44] Hofer J, Schneider T, Singer J M, Willemin M, Keller H, Sasagawa T, Kishio K, Conder K and Karpinski J 2000 *Phys. Rev.* B **62** 631
[45] Meingast Ch, Pasler V, Nagel P, Rykov A, Tajima S and Olsson P 2001 *Phys. Rev. Lett.* **86** 1606
[46] Schneider T and Di Castro D 2004 *Phys. Rev.* B **69** 024502
[47] Schneider T and Keller H 2004 *New J. Phys.* **6** 144
[48] Kleinert H and Schulte-Frohlinde V 2001 *Critical Properties of* $\Phi^4$*-Theories* (Singapore: World Scientific)
[49] Pelissetto A and Vicari E 2002 *Phys. Rep.* **368** 549
[50] Harris A B 1974 *J. Phys. C: Solid State Phys.* **7** 1671
[51] Prange R E 1970 *Phys. Rev.* B **1** 2349
[52] Katayama K *et al* 2003 *Physica* C **388/389** 741
[53] Lortz R, Meingast C, Welp U, Kwok W K and Crabtree G W 2003 *Phys. Rev. Lett.* **90** 237002
[54] Yonezawa S, Muraoka Y, Matsushita Y and Hiori H 2004 *J. Phys. Soc. Japan* **73** 819
[55] Subramanian M A, Aravamudan G and Rao S 1983 *Prog. Solid State Chem.* **15** 55
[56] Hanawa M, Muraoka Y, Tayama T, Sakakibara T, Yamaura J and Hiroi Z 2001 *Phys. Rev. Lett.* **87** 187001
[57] Sakai H, Yoshimura K, Ohno H, Kato H, Kambe S, Walstedt R E, Matsuda T D, Haga Y and Onuki Y 2001 *J. Phys.: Condens. Matter* **13** L785
[58] Jin R, He J, McCall S, Alexander C S, Drymiotis F and Mandrus D 2001 *Phys. Rev.* B **64** 180503
[59] Yonezawa S, Muraoka Y, Matsushita Y and Hiroi Z 2004 *J. Phys.: Condens. Matter* **16** L9
[60] Yonezawa S, Muraoka Y and Hiroi Z 2004 *J. Phys. Soc. Japan* **73** 1655
[61] Brühwiler M, Kazakov S M, Zhigadlo N D, Karpinski J and Batlogg B 2004 *Phys. Rev.* B **70** 020503
[62] Brühwiler M, Kazakov S M, Karpinski J and Batlogg B 2006 *Phys. Rev.* B **73** 094518
[63] Khasanov R, Eshchenko D G, Karpinski J, Kazakov S M, Zhigadlo N D, Brütsch R, Gaville D and Keller H 2004 *Phys. Rev. Lett.* **93** 157004
[64] Khasanov R, Eshchenko D G, Di Castro D, Shengelaya A, La Mattina F, Maisuradze A, Baines C, Luetkens H, Karpinski J, Kazakov S M and Keller H 2004 *Phys. Rev.* B **72** 104504
[65] Schneider T, Khasanov R and Keller H 2005 *Phys. Rev. Lett.* **94** 077002
[66] Kleinert H 1982 *Lett. Nuovo Cimento* **35** 405
[67] Herbut I F and Tesanovic Z 1996 *Phys. Rev. Lett.* **76** 4588
[68] Hove J and Sudbø A 2000 *Phys. Rev. Lett.* **84** 3426
[69] Schneider T, Khasanov R, Conder K, Pomjakushina E, Brütsch R and Keller H 2004 *J. Phys.: Condens. Matter* **16** L437
[70] Kajantie K, Laine M, Neuhaus T, Rajantie A and Rummukainen K 2004 *Nucl. Phys.* B **699** 632
[71] Peskin M E 1978 *Ann. Phys.* **113** 122
Dasgupta C and Halperin B I 1981 *Phys. Rev. Lett.* **47** 1556
Kovner A, Kurzepa P and Rosenstein B 1983 *Mod. Phys. Lett.* A **8** 1343
Kiometzis M, Kleinert H and Schakel A M J 1994 *Phys. Rev. Lett.* **73** 1975
[72] Fisher D S, Fisher M P A and Huse D A 1991 *Phys. Rev.* B **43** 130
[73] Maki K 1965 *Phys. Rev.* **139** A702
[74] Matthias B T *et al* 1954 *Phys. Rev.* **95** 1435
[75] Matthias B T *et al* 1965 *Phys. Rev.* **139** A1501
[76] Testardi L R 1975 *Rev. Mod. Phys.* **47** 637
[77] Frindt R F 1991 *Phys. Rev. Lett.* **28** 299
[78] Soto F H, Berger H, Cabo L, Carballeira C J, Mosqueira J, Pavuna D, Toimil P and Vidal F 2007 *Physica* C **460–462** 789
[79] Kokubo N *et al* 2007 *Phys. Rev.* B **75** 184512
[80] Wang Y *et al* 2005 *Phys. Rev.* B **72** 024548
[81] Lortz R, Wang Y, Demuer A, Böttger M, Bergk B, Zwicknagl G, Nakazawa Y and Wosnitza J 2007 *Phys. Rev. Lett.* **99** 187002
[82] Fulde P and Ferrel R A 1964 *Phys. Rev.* **135** A550
[83] Larkin A I and Ovchinnikov Y N 1964 *Zh. Eksp. Teor. Fiz.* **47** 1136
Larkin A I and Ovchinnikov Y N 1965 *Sov. Phys.—JETP* **20** 762 (Engl. Transl.)
[84] Schneider T 2003 *Phys. Rev.* B **67** 134514
[85] Khasanov R, Schneider T and Keller H 2007 *Phys. Rev.* B **72** 014524